Magnetorheological Fluid Based Braking System using L-shaped Disks

Mohammadhossein Hajiyan, Shohel Mahmud, and Hussein A. Abdullah

School of Engineering, University of Guelph, 50 Stone Road East,
Guelph, Ontario, Canada, N1G 2W1
For correspondence: mhajiyan@uoguelph.ca, Tel: +1(226) 500-0211

Abstract: This paper presents a novel design of multi-disks Magnetorheological braking system (MR brake) for automotive application. Magnetic saturation in both electromagnetic core and MR fluid is considered in this paper. The electromagnetic analysis of the proposed configuration is carried out using Finite Element based COMSOL multiphysics software (AC/DC module). The system geometry, created using AutoCAD software, is discretized using a finite number of triangular elements with a higher concentration of elements near the internal boundaries. Post processing option of COMSOL multiphysics software is utilized to calculate the magnetic field distribution and magnetic flux density inside the MR fluid and electromagnetic core. A one dimensional analytical model is developed to calculate the braking torque of the proposed system. The performance of the proposed design shows improvement over the designs available in the existing literature considering the same dimensional restrictions.

Keywords: Magnetorheological fluid, Braking torque, Finite Element Analysis, Bingham Model.

1. Introduction

Magnetorheological fluids (MR fluid) are a class of smart fluids which are composed of liquids (basically oils) and varying percentages of iron particles. MR fluids are widely being used in applications where controllability and flexibility are important. For instance, in large-scale damper to protect structures [1], damping system for small and mid size applications [2][3][4], Braking systems [5][6][7], portable rehabilitation devices and prosthetic joints [8][9], and body fitness equipment [10]. The two important characteristics of MR fluid are: variable viscosity and fast response. The former characteristic feature depends on the magnitude of the applied magnetic field and the latter can provide semi-solid material within a millisecond as soon as the magnetic field is applied to the MR fluid. Figure 1 will clearly explain the arrangement of iron particles in MR fluid without and with the imposed magnetic field.

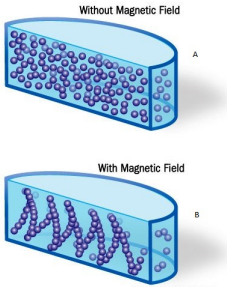

Figure 1: Arrangement of iron particles inside the MR fluid in the absence (A) and presence (B) of magnetic field [11].

2. Related Works

In recent days, MR braking systems have received considerable attention in the automotive industries. However, automotive industries are paying special focus on the generation of higher braking torque using MR braking systems. One of the limitations of MR fluid is its low magnetic permeability com-

pared to the iron core used in MR braking system. Directing an increasing amount of magnetic flux through the MR fluid can provide higher braking torques, which remains as one of the challenging factors during design. For example, Nguyen and Choi [12] proposed braking systems with disk type, drum type, and T-shaped disks. Kwan et al. [13] proposed a new design of MR braking system with small steel roller.

In this paper, we propose a new disk geometry which can direct more magnetic flux into MR fluid compared to the configurations reported in the current literature. The proposed configuration shows the potential to improve the torque produced by the MR brake. Therefore, the major contribution of this paper can be summarized as:

- development of a mathematical model for the proposed design that utilizes Bingham model to calculate the braking torque.
- simulation of the MR brake system using COMSOL multiphysics software.

3. The Proposed Design

This section presents a brief description of the proposed MR braking system. Figure 2 shows the three dimensional CAD drawing of the braking system with its important components. The major components are shown in Figure 3 are : (a) straight and L-shaped disks, (b) cavities filled with MR fluid, (c) back iron, (d) shaft, and (e) copper coil. The flanges on two L-shaped side disks are designed to direct the magnetic field into the MR fluid and consequently increase magnetic field inside the MR fluid. Figure 3 presents the location of the major components of the proposed design. The rational behind selecting the current geometry is to obtain

- maximum possible magnetic field intensity inside the MR fluid within its saturation limit
- higher braking torque

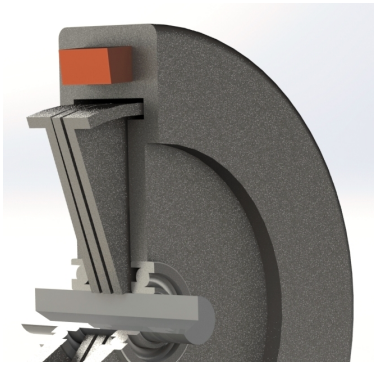

Figure 2: CAD model of the proposed design

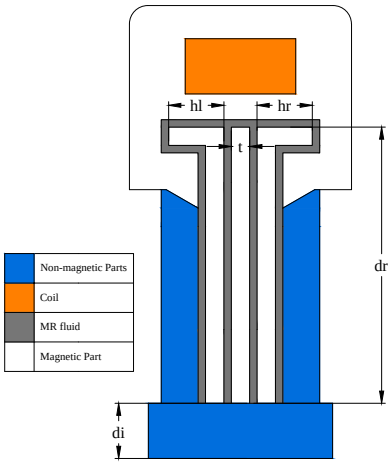

Figure 3: Parameters of the proposed MR braking system.

In this study, some dimensional limitations have been considered to simulate a feasible MR braking system for automotive applications. Table 1 provides some important dimensions to simulate the proposed design in COMSOL software environment.

Table 1: Dimensional limitations of the MR brake.

Parameters	Upper boundary
MR brake diameter	260 mm
MR brake width	60 mm
Assembly clearance	2 mm
Disks thickness	5 mm
MR fluid gap	1 mm

3.1. Material

Table 2 provides the list of materials used for different parts to simulate the MR brake. Note that sealing accessories, such as, screws,

nuts, o-rings, and rotary sealing are disregarded.

Table 2: Material description for the MR brake simulation.

Parts	Material description
Magnetic	AISI-1010
Non-magnetic	AISI-4340
MR fluid	MRF-132DG
Coil	Copper AWG-24

3.2. Torque Equation

This section will present the equations to calculate the output torque of the proposed system. A prior calculation of the magnetic field intensity and identification of the saturation point in different parts of the MR braking system are required for torque calculation. However, the functional relationship between the magnetic flux density (B) and the magnetic field intensity (H) is highly non-linear for most of the magnetic materials which poses some complexity while calculating torque for a particular system. To elaborate on the non-linear magnetic material behaviour, Figure 5 illustrates graphically the functional relationship between B and H of AISI 1010 steel which is the magnetic material selected for the new proposed design. In order to complete the torque model of proposed system MR fluid is treated as a non-Newtonian fluid which obeys Bingham model. For single disk the braking torque is given by

$$T_b = 2\pi N \int_{r_i}^{r_o} (\mu_p \frac{r\omega}{h} + KH^{\beta}) r^2 dr \qquad (1)$$

where N is the number of disks contacting the MR fluid, ω is the angular velocity of the disk and h is the MR fluid gap, K and β are constant parameters and depends on the specific fluid, and r_i and r_o are the inner and the outer radius of brake disks, respectively.

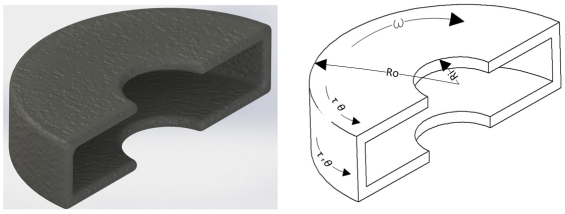

Figure 4: Annular MR fluid in the gap.

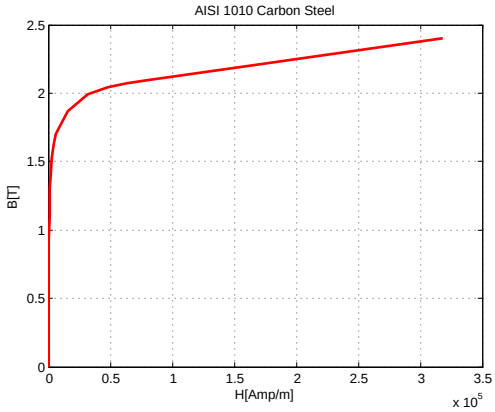

Figure 5: B-H curve for AISI 1010 [7].

Readers are referred to Figure 2 to Figure 4 for the explanation of different dimensions in the torque equation. Now, the generated braking torque for the entire system, as shown in Figure 3, can be calculated from the following equations:

$$T_b = \pi \int_0^{d_r} r^2 \tau dr + \pi r^2 \int_0^{h_l} \tau dr \qquad (2)$$

$$+\pi \int_0^{t} r^2 \tau dr + \pi r^2 \int_0^{h_l - t} \tau dr$$

$$+\pi \int_0^{d_r - t} r^2 \tau dr + 2\pi \int_0^{d_r} r^2 \tau dr + \pi r^2 \int_0^{t} \tau dr$$

$$+\pi \int_0^{d_r} r^2 \tau dr + \pi r^2 \int_0^{h_r} \tau dr$$

$$+\pi \int_0^{t} r^2 \tau dr + \pi r^2 \int_0^{h_r - t} \tau dr + \pi \int_0^{d_r - t} r^2 \tau dr$$

The final torque equation can be obtained after all integrations are performed:

$$T_b = \frac{\pi \tau_H d_r^3}{3} + \frac{\pi \omega \mu_p d_r^4}{4g} + \pi d_r^2 \tau_H h_l \qquad (3)$$

$$+\frac{\pi d_r^2 \omega \mu_p h_l^2}{2g} + \frac{\pi \tau_H t^3}{3} + \frac{\mu_p \omega \mu_p t^4}{4g}$$

$$+\pi(d_r - t)^2 \tau_H (h_l - t) + \frac{\pi (d_r - t)^2 \omega \mu_p (h_l - t)^2}{2g}$$

$$+\frac{\pi \tau_H (d_r - t)^3}{3} + \frac{\pi \omega \mu_p (d_r - t)^4}{4g} + \frac{2\pi \tau_H d_r^3}{3}$$

$$+\frac{\pi \tau_H d_r^3}{3} + \frac{\pi \omega \mu_p d_r^4}{2g} + \pi d_r^2 t \tau_H + \frac{\pi d_r^2 \mu_p \omega t^2}{2g}$$

$$+\frac{\pi \omega \mu_p d_r^4}{4g} + \pi d_r^2 \tau_H h_l + \pi (d_r - t)^2 \tau_H (h_l - t)$$

$$+\frac{\pi d_r^2 \omega \mu_p h_l^2}{2g} + \frac{\pi \tau_H t^3}{3} + \frac{\pi \omega \mu_p (d_r - t)^4}{4g}$$

$$+\frac{\pi (d_r - t)^2 \omega \mu_p (h_l - t)^2}{2g} + \frac{\pi \tau_H (d_r - t)^3}{3} + \frac{\mu_p \omega \mu_p t^4}{4g}$$

It is important to note that T_b(Eq. 3) is a function of τ which can be obtained from the relationship between the yield stress and magnetic field intensity as presented in Figure 6.

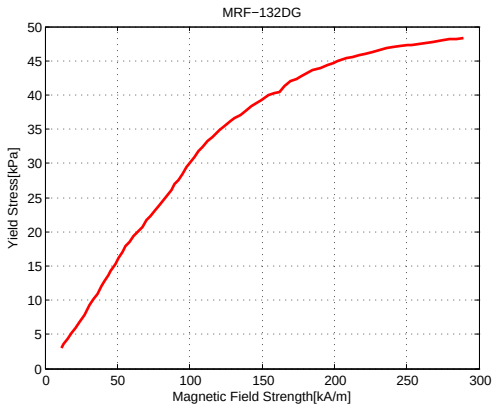

Figure 6: Magnetic field vs. Yield stress [14].

4. Numerical simulations

Magnetic Field module (mf) of COMSOL software (AC/DC module) is selected to simulate the proposed system. In order to reduce computational time, only a 2D axisymmetric section is used for the simulation. To calculate the magnetic field intensity (H) across the shear surfaces, the line and area integrations available in the post-processor of AC/DC module is utilized. Figure 7 presents the mesh used for COMSOL simulation. Mesh size is selected using the COMSOL's automatic mesh generator with "Extra fine" element option. Approximately 8900 triangular elements are used to solve the following electromagnetic equations:

$$J_e = \bigtriangledown \times \ H \tag{4}$$

$$\bigtriangledown \cdot B = 0 \tag{5}$$

The solver was stationary and non-linear in this study. Non-linear material properties are considered for both the MR fluid and magnetic steels. Air boundary around the whole system is selected.

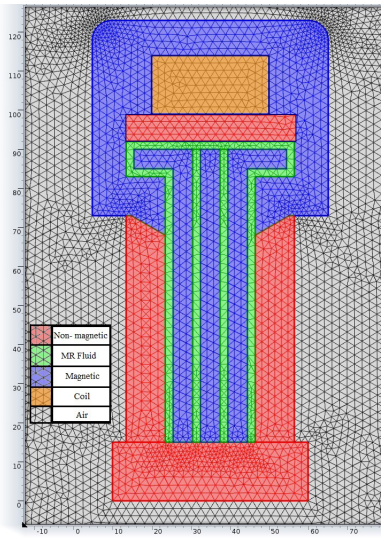

Figure 7: Mesh used for the proposed system using small size triangular element.

5. Result and Discussion

In this section, some simulation results are presented. Figure 8 provides the qualitative surface plot of magnetic flux density in MR brake for applied current density of 10E5 [A/m2]. The magnetic field concentrations around the corners are notable in Figure 8. Magnetic flux leakage in the system increases when higher current density is applied. Therefore, round edges are highly recommended to design the prototype to reduce the magnetic leakage.

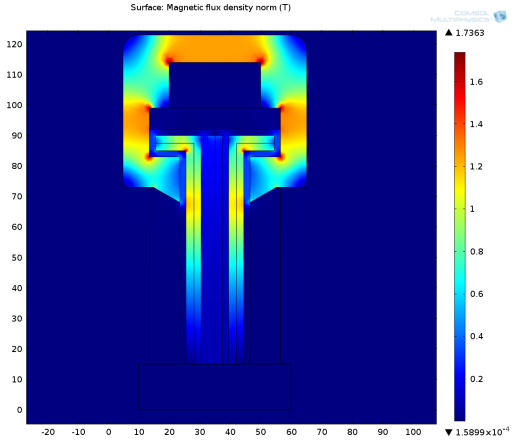

Figure 8: Magnetic flux density of MR brake when current density is $J \approx 20E5$ $[A/m^2]$.

Figure 9 shows the corresponding magnetic vector potential contours inside the braking system. It is observed clearly from the magnetic potential plot in Figure 9 that flanges of side disks direct the magnetic field to MR fluid efficiently. In this design, the generated magnetic flux is higher when the applied current density was lower compared to [15] (Figure 10).

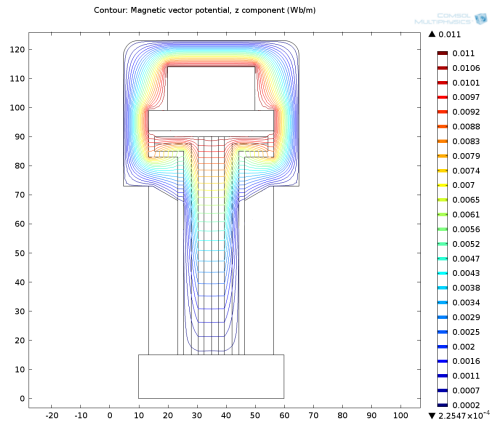

Figure 9: Magnetic vector potential of MR brake when current density is $J \approx 20E5$ $[A/m^2]$.

It is observed from Figure 6 that the yield stress in MR fluid increases with increasing magnetic field. This trend can result in a higher braking torque in the proposed system. However, magnetic saturation in MR fluid has to be taken into account. Figure 10 illustrates the magnetic flux distribution on both the mid and side disks. In Figure 10, a significant difference is observed between the flux around the tip of the disks compared to the root of the disks. It is important to mention that the design considered in this paper is based on ease of manufacturing and machining feasibility.

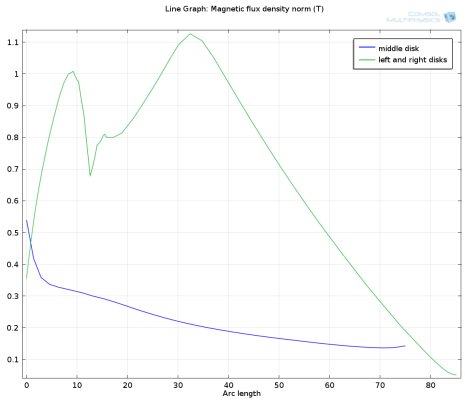

Figure 10: Magnetic flux on disks when current density is $J \approx 20E5$ $[A/m^2]$.

Figure 11 shows the magnetic field intensity distribution in MR fluid. The yield stress can be computed using this distribution and Figure 6. As can be seen from this figure that the maximum magnetic field in the MR braking system is approximately 8E4 A/m.

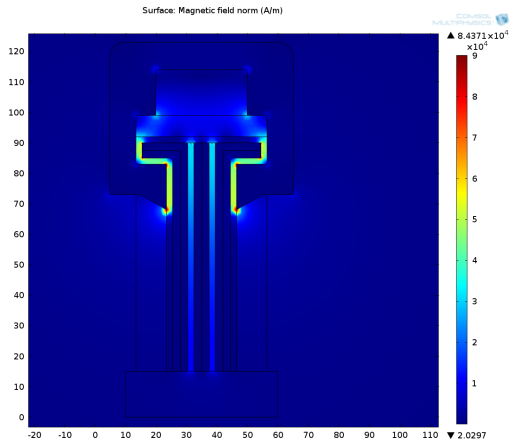

Figure 11: Magnetic field intensity distribution in MR fluid when current density is $J \approx 20E5$ $[A/m^2]$.

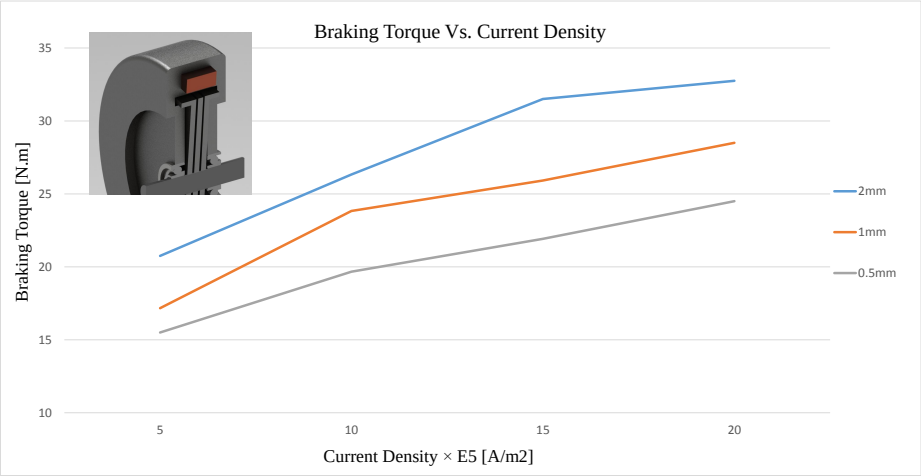

Figure 12: Braking torque vs. Current density with different MR fluid gap.

Figure 12 provides braking torque of the system when different current densities are applied. Three different values of MR fluid gap (i.e., 0.5 mm, 1.0 mm, and 2 mm) are used in Figure 12. It is observed from the figure that a braking system with 2 mm MR fluid gap can generate highest braking torque when the maximum possible current density is approximately $20\times10^5 A/m^2$. Applying a current density beyond this point may cause unwanted heat generation by the coil which results in greater loss throughout the MR braking system.

Finally, the torque generation performance of the proposed system is compared with the performance results presented by Benetti and Dragoni [15]. Note that the system of Benetti and Dragoni [15] consists of 6 rotary and 6 stationary straight disks. Authors obtained an average torque of 8.5 $N.m$ for each discs with an applied current density of 2.5 A/mm^2. In contrast, our 3-disk system can produce total 33 $N.m$ (11 N.m/disc) for the same current density input within the same geometric dimensional restrictions.

6. Conclusion

In this paper, a new geometry of disks in Magnetorheological brake is presented. Analytical models of the system that utilize Bingham model are provided to calculate the braking torque for an applied magnetic field. Furthermore, magnetic field intensity and the magnetic flux density are calculated using finite element based COMSOL software. Nonlinear relationship between magnetic field and magnetic flux for commercially available MR fluid is applied during current simulation. The proposed design shows improvement over the designs available in the current literature with the same limitations.

Remarks on COMSOL

One of the advantages of COMSOL is the use of "material definition" which gives us flexibility to define non-linear relationship between Magnetic flux and Magnetic field. Surface integration tool helps us to compute the magnetic flux on the internal surfaces. Generation of 2D graph in the post-processing mode to illustrate magnetic flux density on the disks is very user friendly. Another advantage of using COMSOL is the easy selection of mesh type, mesh size, and mesh control near corners and interfaces. Finally, COMSOL LiveLink for AutoCad allows us updating the model on COMSOL and re-simulate the system.

References

[1] G. Yang, B. S. Jr., J. D. Carlson, and M. K. Sain, "Large-scale mr fuid dampers: modeling and dynamic performance considerations," *Engineering Structures*, vol. 24 no. 3, pp. 309–323, 2002.

[2] I. Iryani, M. Yazid, S. A. Mazlan, T. Kikuchi, H. Zamzuri, and F. Imaduddin, "Design of magnetorheological damper with a combination of shear and squeeze modes," *Materials and Design*, vol. 54, pp. 87–95, 2014.

[3] D. Ghorbany, "Magnetorehological damper hysteresis characterization for the semi-active suspension system," Master's thesis, University of Agder, 2011.

[4] J. W. Gravatt, "Magneto-rheological dampers for super-sport motorcycle applications," Master's thesis, Virginia Polytechnic Institute and State University, 2003.

[5] C. Sarkar and H. Hirani, "Design of a squeeze film magnetorheological brake considering compression enhanced shear yield stress of magnetorheological fluid," *Electrorheological Fluids and Magnetorheological Suspensions*, vol. 412, p. conference 1, 2012.

[6] O. Erol and H. Gurocak, "Interactive design optimization of magnetorheological-brake actuators using the taguchi method," *Smart Materials and Structures*, vol. 20 no. 10, p. ., 2011.

[7] K. Karakoc, E. J. Park, and A. Suleman, "Design considerations for an automotive magnetorheological brake," *Mechatronics*, vol. 18 no.8, pp. 434–447, 2008.

[8] M. Avraam, M. Horodinca, P. Letier, and A. Preumont, "Portable smart wrist rehabilitation device driven by rotational mr-fluid brake actuator for telemedecine applications," in *International Conference on Intelligent Robots and Systems*, 2008.

[9] F. Jonsdottir, E. T. Thorarinsson, H. Palsson, and K. H. Gudmundsson, "Influence of parameter variations on the braking torque of a magnetorheological prosthetic knee," *Intelligent Material Systems and Structures*, vol. 20, pp. 659–667, 2009.

[10] W. K. Sum, Liao, and W. Hsin, "Adaptive body fitness equipment using magnetorheological fluids," in *ROBIO*, pp. 432–437, IEEE, 2005.

[11] *http://science.howstuffworks.com/*.

[12] Q. H. Nguyen and S. B. Choi, "Selection of magnetorheological brake types via optimal design considering maximum torque and constrained volume," *Smart Materials and Structures*, vol. 21 no. 1, pp. 12–20, 2012.

[13] A. K. Kwan, T. H. Nam, and Y. Young, "New approach to design mr brake using a small steel roller as a large size magnetic particle," in *International Conference on Control, Automation and Systems*, 2008.

[14] *http://www.lord.com/*.

[15] M. Benetti and E. Dragoni, "Nonlinear magnetic analysis of multi-plate magnetorheological brakes and clutches," in *COMSOL Users Conference 2006 Milano*, 2006.